Revision 1

Interaction between composition and temperature effects on non-bridging oxygen and high-coordinated aluminum in calcium aluminosilicate glasses

Linda M. Thompson* and Jonathan F. Stebbins

Department of Geological and Environmental Sciences, Stanford University, Stanford, CA 94305, USA (*lison@stanford.edu)

Abstract

The configurational changes that occur with temperature, and how these vary with composition, affect the thermodynamic and transport properties of aluminosilicate melts but are not well understood. We present here high-resolution ^{27}Al and ^{17}O NMR data on several calcium aluminosilicate glasses along two silica isopleths crossing the metaluminous (SiO_2-$CaAl_2O_4$) join, prepared with varying quench rates and thus with fictive temperatures spanning approximately 100 K. In all compositions, five coordinated aluminum increases with increasing fictive temperature. For glasses along the 60 mol% SiO_2 isopleth, NBO also increases with increasing fictive temperature; this is less obvious for the glasses along the 30 mol% SiO_2 isopleth. The data suggest the mixing of bridging oxygen contributes to the magnitude of the observed temperature effect on NBO and continue to suggest the existence of multiple mechanisms that generate NBO and ^{V}Al.

Keywords: NMR spectroscopy, non-bridging oxygen, five-coordinated aluminum, temperature effects

Introduction

Understanding the structure of aluminosilicate melts and glasses and its impact on their properties has been the subject of much research (see reviews (Mysen and Richet, 2005; Stebbins et al., 1995)) because of their importance to both geological processes (most magmas) and technology (e.g., flat-panel displays). Network connectivity (melt polymerization) in particular has been highlighted as a significant factor in thermodynamic and transport properties (Lee et al., 2004; Lee and Stebbins, 2006) and is often predicted from composition using "standard" models of the melt structure.

These "standard" models of aluminosilicate structure use simple concepts from known crystal structures to approximate the melt structure, assuming that in an ambient-pressure melt with modifier oxides equal to or in excess of alumina (e.g., mol% $Al_2O_3 \leq CaO$ or K_2O), all Al^{3+} cations are four-coordinated (^{IV}Al). Oxygen anions connecting two network formers (e.g., Si^{4+} or Al^{3+}) are described as bridging oxygens, while oxygens coordinated to only one network former are known as non-bridging oxygens (NBO) and rely on network modifiers to compensate the remaining valence charge. Along the metaluminous (charge-compensated) join (e.g., $CaAl_2O_4$-SiO_2), it is assumed that all O atoms are bridging; additional modifier oxide results in the formation of NBO with the concentration predictable by stoichiometry.

It should now be recognized, however, that this "standard" model is only a first approximation and fails to account for several observed structural species that are of relatively low concentration but are potentially important in models of both thermodynamic and transport properties. For example, high-resolution ^{27}Al NMR spectroscopy has demonstrated that, for most glasses in the CaO-Al_2O_3-SiO_2 system, there is significant (4-8%) ^{V}Al, with complex

relationships between concentration and composition (Neuville et al., 2004; Neuville et al., 2006; Stebbins et al., 2000; Thompson and Stebbins, 2011). Significant quantities of ^{V}Al have also been found in ambient-pressure Mg- and alkali aluminosilicates (Allwardt et al., 2005b; McMillan and Kirkpatrick, 1992; Toplis et al., 2000). Evidence from melts quenched at pressures up to 10 GPa has shown that cation field strength (cation size and charge) affects the average Al coordination, with higher field strengths corresponding to increases in the ^{V}Al content (Allwardt et al., 2005b; Allwardt et al., 2007; Kelsey et al., 2009); ambient pressure aluminosilicate and aluminoborate glasses have similar trends (Allwardt et al., 2005b; Florian et al., 2007; Iftekhar et al., 2011; Thompson and Stebbins, 2012).

Similarly to the "non-standard" presence of ^{V}Al, ^{17}O NMR has detected between 1-8% NBO in several compositions along the metaluminous join in the CAS system, where its concentration is predicted to be zero by the "standard" model and therefore its presence requires additional structural changes (such as ^{V}Al and/or three-coordinated oxygen) to maintain local charge balance (Lee and Stebbins, 2006; Oglesby et al., 2002; Stebbins et al., 2008; Stebbins et al., 1999; Stebbins and Xu, 1997). Subsequent work has shown NBO persisting well into the peraluminous compositional region (Thompson and Stebbins, 2011), where its presence was predicted from variations of melt viscosity with composition (Toplis and Dingwell, 2004; Toplis et al., 1997b) and has also been examined by Raman spectroscopy (Mysen and Toplis, 2007). Studies of the potassium aluminosilicate and barium aluminosilicate systems have also found NBO in metaluminous and peraluminous glasses (Thompson and Stebbins, 2011; Thompson and Stebbins, 2012); the limited evidence presented suggests that cation charge has a more important effect on NBO content than does cation radius for a given valence. However, NMR evidence also suggests that in highly peralkaline or peralkaline earth compositions, NBO contents are

consistent with those predicted by stoichiometry (Allwardt et al., 2005a; Stebbins et al., 2008; Thompson et al., 2012).

To apply these data to systems of interest (e.g., melts in geological processes), it remains important to understand what structural changes occur with changing temperature because of the significant configurational component to the heat capacity in most silicate liquids and its consequent role on thermodynamic and transport properties (Mysen and Richet, 2005; Richet, 1984; Richet and Neuville, 1992). These structural changes are often divided into two categories: "topological" changes are characterized as changes in the distribution of bond distances and bond angles while "chemical" changes are characterized as changes in the disordering of cations, anions, and potentially other small structural units on defined "sites" in the overall melt structure (Richet and Neuville, 1992). Although both are likely to be important, the latter have drawn somewhat more interest because they can be more readily estimated and potentially related to thermodynamic properties by simple models of entropies of mixing (Lee and Stebbins, 1999; Toplis, 2001; Toplis et al., 1997a).

Measurements of temperature effects on melt structure have been done either through direct observation of the melt using in situ methods or by investigating glass samples prepared by cooling the melt at different rates. If the melt is rapidly quenched, the structure is "frozen" in at a relatively high temperature (the fictive temperature, T_f) and the glass records a more disordered state than if the melt is slowly cooled, producing a glass with a lower T_f and less disorder. Although laboratory quench rates limit obtainable fictive temperatures to a range of approximately 200 K, this approach allows the application of a wider range of techniques only accessible at ambient temperature, including the most advanced high-resolution NMR spectroscopic methods. Both methods have been used to observe a variety of effects of

increasing temperature on melt structure, as recently summarized (Stebbins, 2008). Comparison to simulated structures from molecular dynamics approaches can also provide some insight, although the high fictive temperatures (> 2000 K) common in such models (due to extreme computational requirements for lower temperature dynamics) requires either extrapolation of experimental data up in temperature or simulated structures down in temperature, reinforcing the need to understand structural changes that occur with changing temperature.

However, temperature effects on aluminosilicate melts are less well-characterized than those in borosilicate and boroaluminosilicate melts, in part due to the higher glass transition temperatures. Early in situ, high temperature X-ray scattering experiments on $CaAl_2Si_2O_8$ and $NaAlSi_3O_8$ melts found no significant changes from the glasses (Marumo and Okuno, 1984; Taylor et al., 1980). Likewise, comparison of early ambient and high temperature ^{27}Al NMR spectra for calcium aluminates (McMillan et al., 1996; Poe et al., 1993) and for calcium aluminosilicates (Coté et al., 1992) found no clear, systematic differences between the glasses and melts. However, in-situ, high-temperature NMR studies of alkali aluminosilicate glasses and melts (Stebbins and Farnan, 1992) and a calcium aluminosilicate (Kanehashi and Stebbins, 2007) have shown shifts in the mean values of the isotropic chemical shift (δ_{iso}) that are consistent with higher concentrations of ^{V}Al at higher temperatures. High-temperature X-ray absorption spectra on $CaAl_2Si_2O_8$ and $CaAl_2O_4$ melts have also been interpreted as showing changes with increasing temperature consistent with an increase in ^{V}Al (Neuville et al., 2008). Support for increasing ^{V}Al content with increasing temperature also comes from ^{27}Al MAS NMR spectra of Al_2O_3-SiO_2 glasses (Poe et al., 1992a; Sato et al., 1991) and a series of calcium aluminosilicate glasses (Stebbins et al., 2008) with varying quench rates. These results are also consistent with the large concentrations of ^{V}Al often seen in molecular dynamics simulations of aluminosilicate

melt structure, although this depends on model potential (Morgan and Spera, 2001; Nevins and Spera, 1998; Poe et al., 1992b; Poole et al., 1995; Scamehorn and Angell, 1991; Stein and Spera, 1995). Drawing comparison to the temperature effects in boron-containing systems is difficult as these are frequently more complex, with increases consistent with aluminosilicate glasses observed in a fictive-temperature study of E-glass (Kiczenski et al., 2005) but slightly decreasing ^{V}Al content with increasing fictive temperatures in another calcium boroaluminosilicate (Wu and Stebbins, 2010) and a lithium boroaluminate glass (Sen et al., 1998).

Temperature effects involving oxygen speciation remain even less well-characterized. It has long been thought that the extent of order/disorder among the tetrahedrally coordinated network formers (here, ^{IV}Al and ^{IV}Si) and therefore among the Si-O-Al, Si-O-Si, and Al-O-Al bridging oxygens is significant to the configurational entropies and heat capacities (Mysen and Richet, 2005; Richet et al., 1990). In a number of sodium-, lithium-, and calcium aluminosilicate glasses, work has been done to quantify the distribution of these species and analyze them with a statistical thermodynamical model, which predicts an increase in disorder at higher temperatures (Lee and Stebbins, 1999; Lee and Stebbins, 2000a). $NaAlSiO_4$ and $LiAlSiO_4$ glasses with varying quench rates have been shown by ^{17}O NMR to have an increasingly random distribution of bridging oxygen with increasing fictive temperature (Dubinsky and Stebbins, 2006). In a $CaAl_2Si_2O_8$ glass with observed "excess" NBO (above that predicted by the "standard" model), a small increase in NBO content was observed with increasing fictive temperature (Stebbins et al., 2008).

Potential temperature effects on NBO content are of particular interest because connections are often made between the formation of NBO and changes in the coordination of the network cations when discussing temperature, compositional, or pressure effects, as recently

reviewed (Stebbins et al., 2013). Evidence suggests that in aluminosilicate systems, the picture is complex; although sensible arguments can be made for coupled formation of NBO and ^{V}Al (Neuville et al., 2006; Stebbins and Xu, 1997; Toplis et al., 1997b), studies of high-pressure, densified glasses have shown a correlation between NBO loss and network cation coordination increase (Allwardt et al., 2005a; Lee, 2004).

In this study, we present experimental data on the effects of fictive temperature on both NBO and ^{V}Al coordination in two series of calcium aluminosilicate glasses crossing the metaluminous join from percalcic (molar $CaO > Al_2O_3$) to peraluminous ($Al_2O_3 > CaO$) compositions. We explore mechanisms that may promote the formation of NBO or ^{V}Al without directly coupling the two and show how the data here are consistent with other known structural changes effected by temperature.

Experimental

The calcium aluminosilicate system was chosen because of the resolution of the NBO and BO peaks in ^{17}O MAS NMR and because the glass-forming region spans a wide range of compositions. As previously described (Thompson and Stebbins, 2011), the base glasses (representing an intermediate cooling rate) were synthesized in 300 mg batches using SiO_2 enriched to approximately 40% ^{17}O. These base glasses were synthesized in Pt crucibles in an argon environment before the crucibles were quenched in water without wetting the glasses (Thompson and Stebbins, 2011). As before, sample labels show the nominal composition, noted as CASx.y.z, where x is the mol % of CaO, y is the mol % of Al_2O_3, and z is the mol % of SiO_2. In addition, values of $R = CaO/(CaO + Al_2O_3)$ were calculated using the compositions as measured by EPMA; these measured compositions are given in Table 1.

To prepare the slow cooled samples, approximately 100 mg of the water-quenched glass was heated above the glass transition temperature, as verified using differential scanning calorimetry, and then cooled at the rate of 10 K per minute in an argon atmosphere. Fast-quenched samples were prepared using 30 to 50 mg of the water-quenched glass in a platinum foil envelope in a colliding-piston rapid-quench apparatus (Kiczenski et al., 2005) using previously described procedures (Dubinsky and Stebbins, 2006). The resulting Pt envelopes ranged from ~110 to 360 μm thick. An isotopically-unenriched sample was checked using electron microprobe to verify that within uncertainties, there were no compositional changes between the water-quenched and fast-quenched samples, with one exception as noted below.

To measure heat capacities for the fictive temperature estimates, a Netzsch DSC 404 was used. For each composition, between 20 to 30 mg of ground glass (which had previously been heated above T_g and cooled at 0.167 K/s) was packed into a platinum crucible for the run, which was done in argon. Each composition also had an associated blank and standard (sapphire) run under the same experimental conditions to allow calculation of the C_p curve (Wu and Stebbins, 2010). Because these glasses had been previously heated and cooled at 0.167 K/s, all three up-scans recorded the glass transition and width of the glass transition region in the C_p curve. Fictive temperatures were calculated using the equation:

$$\frac{\log q_1 - \log q_2}{\frac{1}{T_{f1}} - \frac{1}{T_{f2}}} = -\frac{\Delta H^*}{2.3R} \qquad [1]$$

where q is the cooling rate in K/s, ΔH^* is the activation enthalpy, and R is the ideal gas constant (Moynihan et al., 1976). For all glasses, T_{f1} was taken as the glass transition temperature (T_g) as determined from DSC with a cooling rate q_1 of 0.167 K/s. Cooling rates for water- and fast-quench glasses were estimated as 1±0.5 x 10^2 K/s and 5±4 x 10^4 K/s (Kiczenski et al., 2005). Activation enthalpies for these glasses were calculated from the width of the C_p transition

regions, as described in Moynihan, et al. (1996), with the onset (and end) defined by the intersection of the extrapolated glassy (or liquid) C_p line and the extrapolated rising (or falling) C_p line of the glass transition peak. Equation 1 was then solved for T_{f2} using the calculated activation enthalpy. The fictive temperatures calculated in this way are reported in Table 2. For comparison, the activation enthalpy for the CAS 20.20.60 glass was also estimated by observing the glass transition as a function of heating/cooling rates in the DSC; for this, all heating/cooling rates (q, ranging from 5 to 20 K min^{-1}) are accurately controlled and the observed T_f is equal to the glass transition temperature at that cooling rate (Potuzak et al., 2008). The activation enthalpy calculated this way was consistent with the estimate made using the width of the C_p transition region.

The 1D MAS NMR spectra for both ^{27}Al and ^{17}O were collected with Varian Unity/Inova spectrometers at 18.8 and 14.1 T fields respectively, using Varian/Chemagnetics "T3" probes with 3.2 mm zirconia rotors spinning at 20 kHz, referenced to either aqueous $Al(NO_3)_3$ or ^{17}O-enriched H_2O. All spectra were acquired using a single pulse excitation with pulse widths of about 0.2 μs (for ^{27}Al) or 0.3 μs (for ^{17}O), which corresponds to about 30^0 radio frequency tip angles in the solid. To optimize the signal-to-noise ratio, delays of 0.1 s (for ^{27}Al) and 1 s (for ^{17}O) were used between pulses. No differential relaxation rates were observed between the different sites when longer delay times were tested. Linear back-prediction was used to produce a flat baseline, with identical parameters used for all oxygen and all aluminum spectra, respectively. A minor amount of Gaussian apodization (small enough to avoid any noticeable effects on line shape) was applied to reduce noise. All plotted spectra are normalized to the highest peak maxima, and quantification of oxygen and aluminum speciation was done using the software package Dmfit, as previously described (Massiot et al., 2002; Thompson and Stebbins,

2011); as before, the Czjzek model was used for fitting the bridging oxygen peak because it best reproduces the slightly asymmetric peak shape and allows accurate measurement of the peak areas. However, the fitted NMR parameters are not expected to provide any physically meaningful information for the ^{17}O spectra, as the oxygen coordination number (2) is less than the required coordination number (4) for the Czjzek model (d'Espinose de Lacaillerie et al., 2008). Fit parameters for the ^{27}Al peaks are presented in Table 3 and are consistent with parameters derived from multiple quantum data for glasses of similar compositions, although estimated mean quadrupolar coupling constants tend to be slightly higher in our results (Neuville et al., 2006). The ^{17}O spectra for the water-quench samples presented here were previously published (Thompson and Stebbins, 2011); all other spectra are newly collected for this study.

Results

Oxygen speciation

In all of the glasses studied here, the common feature in the ^{17}O MAS NMR spectra is the large asymmetric peak centered near 50 ppm, attributed to the bridging oxygen (Fig. 1). The second, smaller peak to the high-frequency (left-hand) side of the main peak is assigned to NBO's using data from both crystalline compounds and binary calcium silicate glasses (Allwardt et al., 2003; Stebbins and Xu, 1997). If small amounts of oxygen triclusters (defined here as an oxygen connected to three tetrahedrally-coordinated network formers) are present, quantum calculations and NMR observations show that their ^{17}O peak would be beneath the large BO signal and cannot be resolved (Iuga et al., 2005; Kubicki and Toplis, 2002; Stebbins et al., 2001). However, because we calculate the NBO content as a percentage of total oxygen, this overlap would have no impact on our results.

In both the CASx.y.60 and CASx.y.30 series (Fig. 2), comparisons of samples with similar cooling rates show that the NBO peak decreases with decreasing R value (increasing aluminum content) as previously described for the water-quenched series (Thompson and Stebbins, 2011). The NBO content at a given R value is higher in the CASx.y.30 series than the CASx.y.60 series at all cooling rates, consistent with our previous study and inferences from viscosity data (Thompson and Stebbins, 2011; Toplis and Dingwell, 2004). NBO's were present above the limit of detection (estimated at < 0.5% of total oxygen) in all samples examined here, including peraluminous compositions. In the CAS32.38.30 samples, ^{27}Al NMR (see below) shows the presence of a small amount of corundum. Published data shows that the ^{17}O NMR peak for corundum would lie underneath the main BO peak in the glass (Brun et al., 1970; Walter and Oldfield, 1989), which could result in a slight underestimation of the NBO content, depending on the amount of ^{17}O incorporated into the residual corundum. As discussed for the ^{27}Al NMR results, there is an obvious decrease in the corundum content from the water-quench sample to the fast-quench sample, presumably indicating continued dissolution during re-melting and implying a slight increase in the aluminum content of the glass. We include the spectra for comparison, but the possible change in composition compared to the water-quenched and slow-cooled samples exclude this fast-quench glass from our considerations of T_f on structure.

In the CASx.y.60 series, no significant changes in the BO peaks were observed with increasing fictive temperature. Direct graphical comparison of the spectra for all three compositions show increases in the NBO content with increasing fictive temperature from the slow-cooled to the fast-quench samples; however, the fast-quench and water-quench samples appear to have similar NBO contents. These results suggest that there are real effects of fictive temperature, but they are small and may be non-linear with temperature. The uncertainties in the

254 fits of the spectra are large enough, however, so that differences in NBO contents with T_f are
255 difficult to quantify, i.e. error ranges overlap substantially as shown in Figure 2. These
256 uncertainties have been explored in detail in a recent study of oxygen speciation in binary
257 alkaline earth silicate glasses (Thompson et al., 2012).

258 The peraluminous sample in the CASx.y.30 series (CAS32.38.30) follows the same
259 pattern observed in the CASx.y.60 series, with no changes apparent in the BO peak and a slight
260 increase in the NBO peak with increasing fictive temperature between the slow-cooled and
261 water-quenched samples. However, at the CAS35.35.30 and CAS38.32.30 compositions, the BO
262 peak broadens (by approximately 5 ppm) and shifts to a slightly lower frequency in the fast-
263 quench samples, possibly due to shifts among BO species. An increase in Al-O-Al content
264 would add intensity to that side of the BO peak; as discussed below, increases in these BO
265 species may play a larger role in the lower silica glasses. In these two compositions, any
266 differences in the NBO peak height among the samples with different fictive temperatures are
267 small relative to the noise levels of the spectra and thus cannot be readily detected.

268 *Aluminum speciation*

269 The ^{27}Al MAS NMR spectra all feature a major, asymmetric peak with a partially
270 resolved shoulder on the low-frequency (right-hand) side (Fig. 3). This main peak is assigned to
271 ^{IV}Al with the shoulder (best visible as a break in the slope) assigned to ^{V}Al based on previous
272 studies of similar compositions (Allwardt et al., 2005b; Neuville et al., 2004; Neuville et al.,
273 2006). The intensity of the ^{V}Al peak increases as the composition changes from percalcic to
274 peraluminous at all cooling rates, consistent with previous studies (Stebbins et al., 2008;
275 Thompson and Stebbins, 2011).

None of the ^{27}Al NMR spectra show evidence of crystallization except those for the CAS32.38.30 composition, which has a small, narrow peak at ~15 ppm. Fitting this peak produces NMR parameters consistent with corundum (Ghose and Tsang, 1973; Jakobsen et al., 1989). There is little or no change in the height of this peak between the water-quench and slow-cooled samples when the spectra are collected under the same experimental conditions, suggesting that the corundum content remains constant and therefore does not contribute to variation in the glass composition. However, the fast-quench sample shows a distinctly smaller corundum peak, suggesting that more of this residual phase was melted and that the composition of the glass may have changed slightly. Therefore, for this glass we only have two isocompositional data points with which to evaluate T_f effects.

Comparisons within each composition show small increases in ^{V}Al with increasing fictive temperature (Fig. 4). This is confirmed by the quantitative fitting which shows a clear increase, sufficient to be outside the range of uncertainty for the majority of samples. Comparison of the fits and spectra to previously reported values for the water-quenched samples show that they are consistent (Thompson and Stebbins, 2011).

Discussion

All of the glasses studied here contain NBO's in measurable quantities, consistent with our previous work (Thompson and Stebbins, 2011) and indicating that structure-based models need to account for the presence of NBO even in metaluminous (e.g. the SiO_2-$CaAl_2O_4$ join) compositions, over a range of temperatures. Direct graphical comparisons of the spectra for the samples in the 60 mol% SiO_2 series do suggest an increase in NBO content with increasing fictive temperature, most clearly visible in the peraluminous sample. The spectra for the 30

mol% SiO_2 series are noisier due to lower enrichment and loss of ^{17}O during melting (despite the argon atmosphere) and show peak broadening in the fast-quenched samples not observed in the CASx.y.60 series, but still suggest the possibility of increased NBO with increasing fictive temperature in at least the peraluminous glass. In both cases, the imprecision of the fitting does not allow accurate quantification of the difference (Thompson et al., 2012).

In a previous study, NBO content was observed to increase with increasing fictive temperature in an anorthite glass ($CaAl_2Si_2O_8$ or CAS25.25.50 in the notation used here), but not in a highly percalcic CAS 43.14.43 glass (Stebbins et al., 2008). When compared with our new results, the consistent factor in the glasses that have shown an increase in NBO content with increasing fictive temperature is that these all have "excess" NBO compared to that predicted by the standard model. However, the differences observed between our CASx.y.60 and CASx.y.30 series also indicate that the effects of changing T_f depend on composition in a complex way.

Fictive temperature effects are also clearly observed on the ^{V}Al content, with increasing T_f leading to an increase in ^{V}Al in the glasses studied here. This is consistent with the previously reported increases in similar CAS glasses (Stebbins et al., 2008) as well as in-situ high-temperature ^{27}Al NMR data for a CAS melt showing a decrease in the average isotropic chemical shift for the melt compared to the glass, which was interpreted as consistent with increasing ^{V}Al content (Kanehashi and Stebbins, 2007). Molecular dynamics simulations (which have high fictive temperatures) at 1 GPa have also shown large amounts of ^{V}Al in a $CaAl_2Si_2O_8$ glass (Nevins and Spera, 1998), even when correcting for the effect of pressure on aluminum coordination, which has been studied for glasses of similar compositions (Allwardt et al., 2005b). It is important to note that the effects we discuss here are specific to aluminosilicate glasses and melts; the addition of boron complicates temperature effects because of the interplay between

boron and aluminum coordination, as has been observed by decreasing amounts of ^{V}Al with increasing fictive temperature in some aluminoborosilicates (Wu and Stebbins, 2010).

Both "excess" NBO and ^{V}Al can be considered as low concentration, high-energy structures whose concentrations increase with increasing temperature for energetic and entropic reasons, contributing to configurational heat capacity, enthalpy, and entropy. However, the formation of either species requires additional perturbations to the standard-model network structure; these perturbations must also change with temperature. Understanding what these perturbations are and how they are linked to NBO, ^{V}Al, or both remains an active topic of research. For example, triclusters have been proposed to explain the presence of excess NBO in aluminosilicate melts (Toplis and Dingwell, 2004; Toplis et al., 1997b). However, it is also possible to write reactions where NBO and ^{V}Al are produced simultaneously, given here using a previously described notation for oxygen speciation (Stebbins et al., 2008), with Si-O-Al bridging oxygens on the left side and ^{V}Al, Si-O-Si and NBO on the right:

$$8[\text{O-Si}_{1/4}\text{Al}_{1/4}]^{1/4-} \Leftrightarrow 10/3[\text{O-3Al}_{1/5}]^{1/5-} + 10/3[\text{O-2Si}_{1/4}]^{0} + 4/3[\text{O-Si}_{1/4}]^{1-} \quad [2]$$

An increase in Si-O-Al bridging oxygen, as would be expected from an increase in the Al/Si ratio, could shift this reaction to the right, increasing the observed NBO and ^{V}Al content – matching the observed behavior of NBO and ^{V}Al on the metaluminous join in the CAS system (Thompson and Stebbins, 2011).

Previous work has shown, however, that no single reaction has been able to match the relative proportions observed for NBO and ^{V}Al or their changes with temperature, suggesting that multiple equilibria must be involved in the formation of these species (Stebbins et al., 2008; Thompson and Stebbins, 2011; Thompson and Stebbins, 2012). The data collected here continue to support this conclusion. Additionally, the wider compositional range studied here provides

345 new insight into the potential compositional effects on these equilibria and how various
346 temperature effects interact.

347 The effect of temperature on the distribution of bridging oxygen (Si-O-Si, Al-O-Al and
348 Si-O-Al) has previously been characterized in $NaAlSiO_4$ and $LiAlSiO_4$ glasses using ^{17}O
349 3QMAS NMR (Dubinsky and Stebbins, 2006). With increasing fictive temperature, the
350 equilibrium:

351 $$2[O\text{-}Si_{1/4}Al_{1/4}]^{0.25-} \Leftrightarrow [O\text{-}2Si_{1/4}]^{0} + [O\text{-}2Al_{1/4}]^{0.5-} \quad [3]$$

352 shifts to the right hand side in alkali and alkaline earth aluminosilicates, as expected from the ΔH
353 > 0 predicted for this equation by a statistical thermodynamic model (Lee and Stebbins, 1999;
354 Lee and Stebbins, 2000a; Lee and Stebbins, 2000b). The shift in this equilibrium will also affect
355 reactions such as reaction 2 (above) in ways dependent on composition and the ΔH of the various
356 reactions. For example, the more localized negative charge on the Al-O-Al may allow the
357 oxygen to better compensate for the localized positive charge of the network modifier; this could
358 reduce the energetic drive to form NBO, especially for the more highly charged modifier cations,
359 which have increased NBO contents (Thompson and Stebbins, 2011; Thompson and Stebbins,
360 2012). Unfortunately, although alkaline earth aluminosilicate glasses have the most "excess"
361 NBO, it is difficult to accurately determine BO speciation in them due to peak overlaps in the
362 3QMAS spectra (Lee and Stebbins, 2000b).

363 As previously noted (Stebbins et al., 2008), it is also possible to produce ^{V}Al
364 independently of NBO through reactions such as:

365 $$4[O\text{-}Si_{1/4}Al_{1/4}]^{0.25-} \Leftrightarrow 2[O\text{-}Si_{1/4}Al_{1/5}]^{0.4-} + [O\text{-}3Al_{1/5}]^{0.2-} + [O\text{-}2Si_{1/4}]^{0} \quad [4]$$

366 The data here (a minimal T_f effect on NBO content in high Al/Si glasses) indicate that this type
367 of reaction may become more important as the Al/Si ratio increases. When changing the

368 temperature or pressure of a melt, an increase in network cation coordination must be
369 accompanied by an increase in oxygen coordination by the network cations because there are no
370 "new" oxygens added (Stebbins et al., 2008). This can be accomplished by transforming an
371 NBO into a BO (as is commonly seen in aluminoborosilicates upon the initial addition of boron)
372 or a BO into a 3-coordinated oxygen (as shown above) or triclusters of three AlO_4 tetrahedral.
373 Future measurements of changes in BO distribution, NBO content, and ^{V}Al content and how they
374 simultaneously vary with temperature may provide additional insight into how reactions such as
375 these interact.
376

377 **Acknowledgements**

378 This research was supported by the National Science Foundation, EAR 1019596. We
379 thank J. Puglisi and C. Liu for access to the 18.8 T NMR spectrometer in the Stanford Magnetic
380 Resonance Laboratory, Bob Jones for assistance with the EMPA analyses, and Jingshi Wu for
381 thoughtful discussion and comments. We are grateful to the comments of the two anonymous
382 reviewers, which improved and clarified this manuscript.
383

384 **References**

385 Allwardt, J.R., Lee, S.K., and Stebbins, J.F. (2003) Bonding preferences of non-bridging O
386 atoms; evidence from ^{17}O MAS and 3QMAS NMR on calcium aluminate and low-silica
387 Ca-aluminosilicate glasses. American Mineralogist, 88, 949-954.
388 Allwardt, J.R., Stebbins, J.F., Schmidt, B.C., and Frost, D.J. (2005a) The effect of composition,
389 compression, and decompression on the structure of high pressure aluminosilicate
390 glasses: an investigation utilizing ^{17}O and ^{27}Al NMR. In J. Chen, Y. Wang, T.S. Duffy,

G. Shen, and L.F. Dobrzhinetskaya, Eds. Frontiers of High Pressure Research, p. 211-240. Elsevier, Amsterdam.

Allwardt, J.R., Stebbins, J.F., Schmidt, B.C., Frost, D.J., Withers, A.C., and Hirschmann, M.M. (2005b) Aluminum coordination and the densification of high-pressure aluminosilicate glasses. American Mineralogist, 90, 1218-1222.

Allwardt, J.R., Stebbins, J.F., Terasaki, H., Du, L.-S., Frost, D.J., Withers, A.C., Hirschmann, M.M., Suzuki, A., and Ohtani, E. (2007) Effect of structural transitions on properties of high-pressure silicate melts; ^{27}Al NMR, glass densities, and melt viscosities. American Mineralogist, 92, 1093-1104.

Brun, E., Derighetti, B., Hundt, E.E., and Niebuhr, H.H. (1970) NMR of ^{17}O in ruby with dynamic polarization techniques. Physics Letters A, 31, 416-417.

Coté, B., Massiot, D., Taulelle, F., and Coutures, J.-P. (1992) ^{27}Al NMR spectroscopy of aluminosilicate melts and glasses. Chemical Geology, 96, 367-370.

d'Espinose de Lacaillerie, J.-B., Fretigny, C., and Massiot, D. (2008) MAS NMR spectra of quadrupolar nuclei in disordered solids: The Czjzek model. Journal of Magnetic Resonance, 192, 244-251.

Dubinsky, E.V., and Stebbins, J.F. (2006) Quench rate and temperature effects on framework ordering in aluminosilicate melts. American Mineralogist, 91, 753-761.

Florian, P., Sadiki, N., Massiot, D., and Coutures, J.P. (2007) ^{27}Al NMR study of the structure of lanthanum- and yttrium-based aluminosilicate glasses and melts. The Journal of Physical Chemistry B, 111, 9747-9757.

Ghose, S., and Tsang, T. (1973) Structural dependence of quadrupole coupling constant e^2qQ/h for ^{27}Al and crystal field parameter D for Fe^{3+} in aluminosilicates. American Mineralogist, 58, 748-755.

Iftekhar, S., Grins, J., Gunawidjaja, P.N., and Edén, M. (2011) Glass formation and structure–property–composition relations of the RE_2O_3–Al_2O_3–SiO_2 (RE=La, Y, Lu, Sc) systems. Journal of the American Ceramic Society, 94, 2429-2435.

Iuga, D., Morais, C., Gan, Z., Neuville, D.R., Cormier, L., and Massiot, D. (2005) NMR heteronuclear correlation between quadrupolar nuclei in solids. Journal of the American Chemical Society, 127, 11540-11541.

Jakobsen, H.J., Skibsted, J., Bildsoe, H., and Nielsen, N.C. (1989) Magic-angle spinning NMR spectra of satellite transitions for quadrupolar nuclei in solids. Journal of Magnetic Resonance, 85, 173-180.

Kanehashi, K., and Stebbins, J.F. (2007) In situ high temperature ^{27}Al NMR study of structure and dynamics in a calcium aluminosilicate glass and melt. Journal of Non-Crystalline Solids, 353, 4001-4010.

Kelsey, K.E., Stebbins, J.F., Singer, D.M., Brown, G.E., Mosenfelder, J.L., and Asimow, P.D. (2009) Cation field strength effects on high pressure aluminosilicate glass structure: Multinuclear NMR and La XAFS results. Geochimica Et Cosmochimica Acta, 73, 3914-3933.

Kiczenski, T.J., Du, L.S., and Stebbins, J.F. (2005) The effect of fictive temperature on the structure of E-glass: a high resolution, multinuclear NMR study. Journal of Non-Crystalline Solids, 351, 3571-3578.

Kubicki, J.D., and Toplis, M.J. (2002) Molecular orbital calculations on aluminosilicate tricluster molecules: Implications for the structure of aluminosilicate glasses. American Mineralogist, 87, 668-678.

Lee, S.K. (2004) Structure of silicate glasses and melts at high pressure: Quantum chemical calculations and solid-state NMR. Journal of Physical Chemistry B, 108, 5889-5900.

Lee, S.K., Cody, G.D., Fei, Y., and Mysen, B.O. (2004) Nature of polymerization and properties of silicate melts and glasses at high pressure. Geochimica et Cosmochimica Acta, 68, 4189-4200.

Lee, S.K., and Stebbins, J.F. (1999) The degree of aluminum avoidance in aluminosilicate glasses. American Mineralogist, 84, 937-945.

Lee, S.K., and Stebbins, J.F. (2000a) Al-O-Al and Si-O-Si sites in framework aluminosilicate glasses with Si/Al=1: quantification of framework disorder. Journal of Non-Crystalline Solids, 270, 260-264.

Lee, S.K., and Stebbins, J.F. (2000b) The structure of aluminosilicate glasses: High-resolution ^{17}O and ^{27}Al MAS and 3QMAS NMR study. The Journal of Physical Chemistry B, 104, 4091-4100.

Lee, S.K., and Stebbins, J.F. (2006) Disorder and the extent of polymerization in calcium silicate and aluminosilicate glasses; O-17 NMR results and quantum chemical molecular orbital calculations. Geochimica et Cosmochimica Acta, 70, 4275-4286.

Marumo, F., and Okuno, M. (1984) X-ray structural studies of molten silicates: anorthite and albite melts. In I. Sunagawa, Ed. Materials Science of the Earth's Interior, p. 25-38. Terra Scientific Publishing Co., Tokyo.

Massiot, D., Fayon, F., Capron, M., King, I., Le Calvé, S., Alonso, B., Durand, J.O., Bujoli, B., Gan, Z., and Hoatson, G. (2002) Modelling one and two-dimensional solid-state NMR spectra. Magnetic Resonance in Chemistry, 40, 70-76.

McMillan, P., Petuskey, W.T., Coté, B., Massiot, D., Landron, C., and Coutures, J.P. (1996) A structural investigation of CaO-Al_2O_3 glasses via ^{27}Al MAS-NMR. Journal of Non-Crystalline Solids, 195, 261-271.

McMillan, P.F., and Kirkpatrick, R.J. (1992) Al coordination in magnesium aluminosilicate glasses. American Mineralogist, 77, 898-900.

Morgan, N.A., and Spera, F.J. (2001) Glass transition, structural relaxation, and theories of viscosity: a molecular dynamics study of amorphous $CaAl_2Si_2O_8$. Geochimica et Cosmochimica Acta, 65, 4019-4041.

Moynihan, C.T., Lee, S.K., Tatsumisago, M., and Minami, T. (1996) Estimation of activation energies for structural relaxation and viscous flow from DTA and DSC experiments. Thermochimica Acta, 280–281, 153-162.

Moynihan, C.T., Macedo, P.B., Montrose, C.J., Gupta, P.K., DeBolt, M.A., Dill, J.F., Dom, B.E., Drake, P.W., Easteal, A.J., Elterman, P.B., Moeller, R.P., Sasabe, H., and Wilder, J.A. (1976) Structural relaxation in vitreous materials. Annals of New York Academy of Science, 279, 15-35.

Mysen, B.O., and Richet, P. (2005) Silicate Glasses and Melts, Properties and Structure. Elsevier, Amsterdam.

Mysen, B.O., and Toplis, M.J. (2007) Structural behavior of Al^{3+} in peralkaline, metaluminous, and peraluminous silicate melts and glasses at ambient pressure. American Mineralogist, 92, 933-946.

Neuville, D.R., Cormier, L., De Ligny, D., Roux, J., Flank, A.-M., and Lagarde, P. (2008) Environments around Al, Si, and Ca in aluminate and aluminosilicate melts by X-ray absorption spectroscopy at high temperature. American Mineralogist, 93, 228-234.

Neuville, D.R., Cormier, L., and Massiot, D. (2004) Al environment in tectosilicate and peraluminous glasses: A ^{27}Al MQ-MAS NMR, Raman, and XANES investigation. Geochimica et Cosmochimica Acta, 68, 5071-5079.

Neuville, D.R., Cormier, L., and Massiot, D. (2006) Al coordination and speciation in calcium aluminosilicate glasses: Effects of composition determined by ^{27}Al MQ-MAS NMR and Raman spectroscopy. Chemical Geology, 229, 173-185.

Nevins, D., and Spera, F.J. (1998) Molecular dynamics simulations of molten $CaAl_2Si_2O_8$: dependence of structure and properties on pressure. American Mineralogist, 83, 1220-1230.

Oglesby, J.V., Zhao, P., and Stebbins, J.F. (2002) Oxygen sites in hydrous aluminosilicate glasses: the role of Al-O-Al and H_2O. Geochimica et Cosmochimica Acta, 66, 291-301.

Poe, B., McMillan, P., Coté, B., Massiot, D., and Coutures, J.P. (1993) $MgAl_2O_4$ and $CaAl_2O_4$ liquids: in-situ high temperature ^{27}Al NMR spectroscopy. Science, 259, 786-788.

Poe, B.T., McMillan, P.F., Angell, C.A., and Sato, R.K. (1992a) Al and Si coordination in SiO_2-Al_2O_3 glasses and liquids: A study by NMR and IR spectroscopy and MD simulations. Chemical Geology, 96, 333-349.

Poe, B.T., McMillan, P.F., Coté, B., Massiot, D., and Coutures, J.P. (1992b) Silica-alumina liquids: in-situ study by high-temperature aluminum-27 NMR spectroscopy and molecular dynamics simulation. The Journal of Physical Chemistry, 96, 8220-8224.

Poole, P.H., McMillan, P.F., and Wolf, G.H. (1995) Computer simulations of silicate melts. In J.F. Stebbins, P.F. McMillan, and D.B. Dingwell, Eds. Structure, dynamics and properties of silicate melts, p. 563-616. Mineralogical Society of America, Washington, DC.

Potuzak, M., Nichols, A.R.L., Dingwell, D.B., and Clague, D.A. (2008) Hyperquenched volcanic glass from Loihi Seamount, Hawaii. Earth and Planetary Science Letters, 270, 54-62.

Richet, P. (1984) Viscosity and configurational entropy of silicate melts. Geochimica et Cosmochimica Acta, 48, 471-483.

Richet, P., and Neuville, D.R. (1992) Thermodynamics of silicate melts: Configurational properties. In S.K. Saxena, Ed. Thermodynamic data: Systematics and estimation. Springer-Verlag, New York.

Richet, P., Robie, R.A., Rogez, J., Hemingway, B.S., Courtial, P., and Tequi, C. (1990) Thermodynamics of open networks: ordering and entropy in $NaAlSiO_4$ glass, liquid, and polymorphs. Physics and Chemistry of Minerals, 17, 385-393.

Sato, R.K., McMillan, P., Dennison, P., and Dupree, R. (1991) High resolution ^{27}Al and ^{29}Si MAS NMR investigation of SiO_2-Al_2O_3 glasses. Journal of Physical Chemistry, 95, 4484.

Scamehorn, C.A., and Angell, C.A. (1991) Viscosity-temperature relations and structure in fully polymerized aluminosilicate melts from ion dynamics simulations. Geochimica et Cosmochimica Acta, 55, 721-730.

Sen, S., Xu, Z., and Stebbins, J.F. (1998) Temperature dependent structural changes in borate, borosilicate and boroaluminate liquids: high-resolution ^{11}B, ^{29}Si and ^{27}Al NMR studies. Journal of Non-Crystalline Solids, 226, 29-40.

Stebbins, J.F. (2008) Temperature effects on the network structure of oxide melts and their consequences for configurational heat capacity. Chemical Geology, 256, 80-91.

Stebbins, J.F., Dubinsky, E.V., Kanehashi, K., and Kelsey, K.E. (2008) Temperature effects on non-bridging oxygen and aluminum coordination number in calcium aluminosilicate glasses and melts. Geochimica et Cosmochimica Acta, 72, 910-925.

Stebbins, J.F., and Farnan, I. (1992) Effects of high temperature on silicate liquid structure; a multinuclear NMR study. Science, 255, 586-589.

Stebbins, J.F., Kroeker, S., Lee, S.K., and Kiczenski, T.J. (2000) Quantification of five- and six-coordinated aluminum ions in aluminosilicate and fluoride-containing glasses by high-field, high-resolution Al-27 NMR. Journal of Non-Crystalline Solids, 275, 1-6.

Stebbins, J.F., Lee, S.K., and Oglesby, J.V. (1999) Al-O-Al oxygen sites in crystalline aluminates and aluminosilicate glasses; high-resolution oxygen-17 NMR results. American Mineralogist, 84, 983-986.

Stebbins, J.F., McMillan, P.F., and Dingwell, D.B. (1995) Structure, dynamics and properties of silicate melts. Mineralogical Society of America, Washington, DC.

Stebbins, J.F., Oglesby, J.V., and Kroeker, S. (2001) Oxygen triclusters in crystalline $CaAl_4O_7$ (grossite) and in calcium aluminosilicate glasses: ^{17}O NMR. American Mineralogist, 86, 1307-1311.

Stebbins, J.F., Wu, J., and Thompson, L.M. (2013) Interactions between network cation coordination and non-bridging oxygen abundance in oxide glasses and melts: Insights from NMR spectroscopy. Chemical Geology, 346, 34-46.

Stebbins, J.F., and Xu, Z. (1997) NMR evidence for excess non-bridging oxygen in an aluminosilicate glass. Nature, 390, 60-62.

Stein, D.J., and Spera, F.J. (1995) Molecular dynamics simulations of liquids and glasses in the system $NaAlSiO_4$-SiO_2: methodology and melt structure. American Mineralogist, 80, 417-431.

Taylor, M., Brown Jr, G.E., and Fenn, P.M. (1980) Structure of mineral glasses--III. $NaAlSi_3O_8$ supercooled liquid at 805°C and the effects of thermal history. Geochimica et Cosmochimica Acta, 44, 109-117.

Thompson, L.M., McCarty, R.J., and Stebbins, J.F. (2012) Estimating accuracy of ^{17}O NMR measurements in oxide glasses: Constraints and evidence from crystalline and glassy calcium and barium silicates. Journal of Non-Crystalline Solids, 358, 2999-3006.

Thompson, L.M., and Stebbins, J.F. (2011) Non-bridging oxygen and high-coordinated aluminum in metaluminous and peraluminous calcium and potassium aluminosilicate glasses: High-resolution ^{17}O and ^{27}Al MAS NMR results. American Mineralogist, 96, 841-853.

Thompson, L.M., and Stebbins, J.F. (2012) Non-stoichiometric non-bridging oxygens and five-coordinated aluminum in alkaline earth aluminosilicate glasses: Effect of modifier cation size. Journal of Non-Crystalline Solids, 358, 1783-1789.

Toplis, M.J. (2001) Quantitative links between microscopic properties and viscosity of liquids in the system SiO_2-Na_2O. Chemical Geology, 174, 321-331.

Toplis, M.J., and Dingwell, D.B. (2004) Shear viscosities of CaO-Al_2O_3-SiO_2 and MgO-Al_2O_3-SiO_2 liquids: implications for the structural role of aluminium and the degree of polymerisation of synthetic and natural aluminosilicate melts. Geochimica et Cosmochimica Acta, 68, 5169-88.

Toplis, M.J., Dingwell, D.B., Hess, K.U., and Lenci, T. (1997a) Viscosity, fragility, and configurational entropy of melts along the join SiO_2-$NaAlSiO_4$. American Mineralogist, 82, 979-990.

Toplis, M.J., Dingwell, D.B., and Lenci, T. (1997b) Peraluminous viscosity maxima in Na_2O-Al_2O_3-SiO_2 liquids: The role of triclusters in tectosilicate melts. Geochimica et Cosmochimica Acta, 61, 2605-2612.

Toplis, M.J., Kohn, S.C., Smith, M.E., and Poplett, I.J.F. (2000) Fivefold-coordinated aluminum in tectosilicate glasses observed by triple quantum MAS NMR. American Mineralogist, 85, 1556-1560.

Walter, T.H., and Oldfield, R. (1989) Magic angle spinning oxygen-17 NMR of aluminum oxides and hydroxides. Journal of Physical Chemistry, 93, 6744-6751.

Wu, J., and Stebbins, J.F. (2010) Quench rate and temperature effects on boron coordination in aluminoborosilicate melts. Journal of Non-Crystalline Solids, 356, 2097-2108.

583
584 **Figures**

585 **Figure 1:** ^{17}O MAS NMR spectra (14.1 T) for CAS glasses along the isopleths (a) 60 mol% SiO_2
586 and (b) 30 mol% SiO_2. Line color corresponds to cooling rate (and therefore T_f): red is fast-
587 quenched, purple is water-quenched, and blue is slow-cooled. Values of R = CaO/(CaO +
588 Al_2O_3), based on EPMA analyses, are shown below the nominal compositions. The * marks the
589 spinning sideband for the natural-abundance ^{17}O signal from the zirconia rotor.

590

591 **Figure 2:** NBO content of each glass (as a % of total O) along the isopleths 60 mol% SiO_2
592 (circles, lower data set) and 30 mol% SiO_2 (squares, upper data set). Point color corresponds to
593 cooling rate (and therefore T_f): red is fast-quenched, purple is water-quenched, and blue is slow-
594 cooled. For each glass composition, the R value is the same, but points have been slightly offset
595 for clarity. Data points for the peraluminous glasses are to the right.

596

597 **Figure 3:** ^{27}Al MAS NMR spectra (18.8 T) for CAS glasses along the isopleths (a) 60 mol%
598 SiO_2 and (b) 30 mol% SiO_2. Line color corresponds to cooling rate (and therefore T_f): red is
599 fast-quenched, purple is water-quenched, and blue is slow-cooled. Values of R = CaO/(CaO +
600 Al_2O_3), based on EPMA analyses, are shown below the nominal compositions. The * marks the
601 spinning sideband; 'c' marks the location of the corundum peak.

602

603 **Figure 4:** ^{V}Al content of each glass (as a % of total Al) along the isopleths (a) 60 mol% SiO_2 and
604 (b) 30 mol% SiO_2. Point color corresponds to cooling rate (and therefore T_f): red is fast-
605 quenched, purple is water-quenched, and blue is slow-cooled. For each glass composition, the R

606 value is the same, but points have been slightly offset for clarity. Data points for the
607 peraluminous glasses are to the right.
608

609

610 **Tables**

611 **Table 1:** Analyzed compositions of CASx.y.z glasses, in mol %.

Sample	**CaO***	**Al_2O_3 ***	**SiO_2 ***	**R**[†]
CAS22.18.60	22.3	17.4	60.3	0.56
CAS20.20.60	19.8	20.2	60.0	0.49
CAS18.22.60	17.1	21.5	61.4	0.44
CAS38.32.30	36.7	31.9	31.5	0.54
CAS35.35.30	33.9	34.5	31.5	0.49
CAS32.38.30[‡]	31.2	37.1	31.7	0.46

* Analyses made with electron microprobe, excluding crystals where present. Error range on all values estimated at ±0.5 mole %.

[†] R value is equal to CaO/(CaO + Al_2O_3). Error range is ±0.01.

[‡] Minor amounts of crystals present in the glass (residual) identified as corundum by ^{27}Al NMR.

612

613

614

615 **Table 2:** Estimated fictive temperatures and ^{V}Al and NBO concentrations.

Sample	**R***	**T_f (K)**	**$^{V}Al/Al_{tot}$†**	**NBO/O_{tot}‡**
CAS22.18.60	0.56	1109±1	0.017	0.049
		1174±10	0.018	0.060
		1242±20	0.021	0.051
CAS20.20.60	0.49	1133±1	0.023	0.022
		1194±10	0.036	0.029
		1261±20	0.043	0.026
CAS18.22.60	0.44	1140±1	0.049	0.009
		1200±10	0.059	0.012
		1263±20	0.069	0.010
CAS38.32.30	0.54	1119±1	0.043	0.095
		1170±10	0.049	0.096
		1225±20	0.058	0.103
CAS35.35.30	0.49	1120±1	0.055	0.054
		1174±10	0.061	0.060
		1231±20	0.078	0.060
CAS32.38.30§	0.46	1124±1	0.081	0.030
		1176±10	0.084	0.044
		1232±20	0.098	0.047

* R value is equal to $CaO/(CaO + Al_2O_3)$. Error range is ±0.01.

† Error range is ±0.005, estimated from variations in visual evaluation of the fit.

‡ Error range is ±0.008, per Thompson et al., 2012.

§ Presence of corundum crystals verified by ^{27}Al NMR.

616

617

618

Table 3: Fit parameters for Al peaks: δ_{iso} is the mean isotropic chemical shift, dCS the range in chemical shift, and C_Q the mean quadrupolar coupling constant.

Sample	Cooling Rate	Peak	δ_{iso} (ppm)	dCS (ppm)	C_Q (MHz)
CAS18.22.60	slow	^{IV}Al	63.3	14.0	8.2
		^{V}Al	34.1	10.0	8.8
	water	^{IV}Al	63.3	14.0	8.2
		^{V}Al	34.1	10.0	8.8
	fast	^{IV}Al	63.3	14.0	8.2
		^{V}Al	34.1	10.0	8.8
CAS20.20.60	slow	^{IV}Al	63.2	13.9	7.7
		^{V}Al	34.2	6.9	8.9
	water	^{IV}Al	63.2	13.9	7.7
		^{V}Al	34.2	6.9	8.9
	fast	^{IV}Al	63.2	13.9	7.7
		^{V}Al	34.2	6.9	8.9
CAS22.18.60	slow	^{IV}Al	63.4	13.1	7.5
		^{V}Al	30.2	4.8	8.7
	water	^{IV}Al	63.4	13.1	7.5
		^{V}Al	30.4	6.9	8.9
	fast	^{IV}Al	63.6	13.4	7.7
		^{V}Al	30.8	6.9	8.9
CAS32.38.30	slow	^{IV}Al	71.5	13.5	8.0
		^{V}Al	40.2	10.1	8.8
	water	^{IV}Al	71.5	13.4	8.0
		^{V}Al	40.1	10.8	8.2
	fast	^{IV}Al	71.5	13.7	8.2
		^{V}Al	41.8	10.1	9.0
CAS35.35.30	slow	^{IV}Al	72.3	13.1	8.0
		^{V}Al	39.9	8.6	8.9
	water	^{IV}Al	72.3	13.1	8.0
		^{V}Al	40.5	8.6	8.9
	fast	^{IV}Al	71.9	13.8	8.1
		^{V}Al	40.6	14.5	8.7
CAS38.32.30	slow	^{IV}Al	72.8	13.2	7.9
		^{V}Al	39.6	8.6	8.9
	water	^{IV}Al	72.3	13.1	8.0
		^{V}Al	40.5	8.6	8.9
	fast	^{IV}Al	72.6	13.5	8.1
		^{V}Al	40.7	8.8	9.7

619

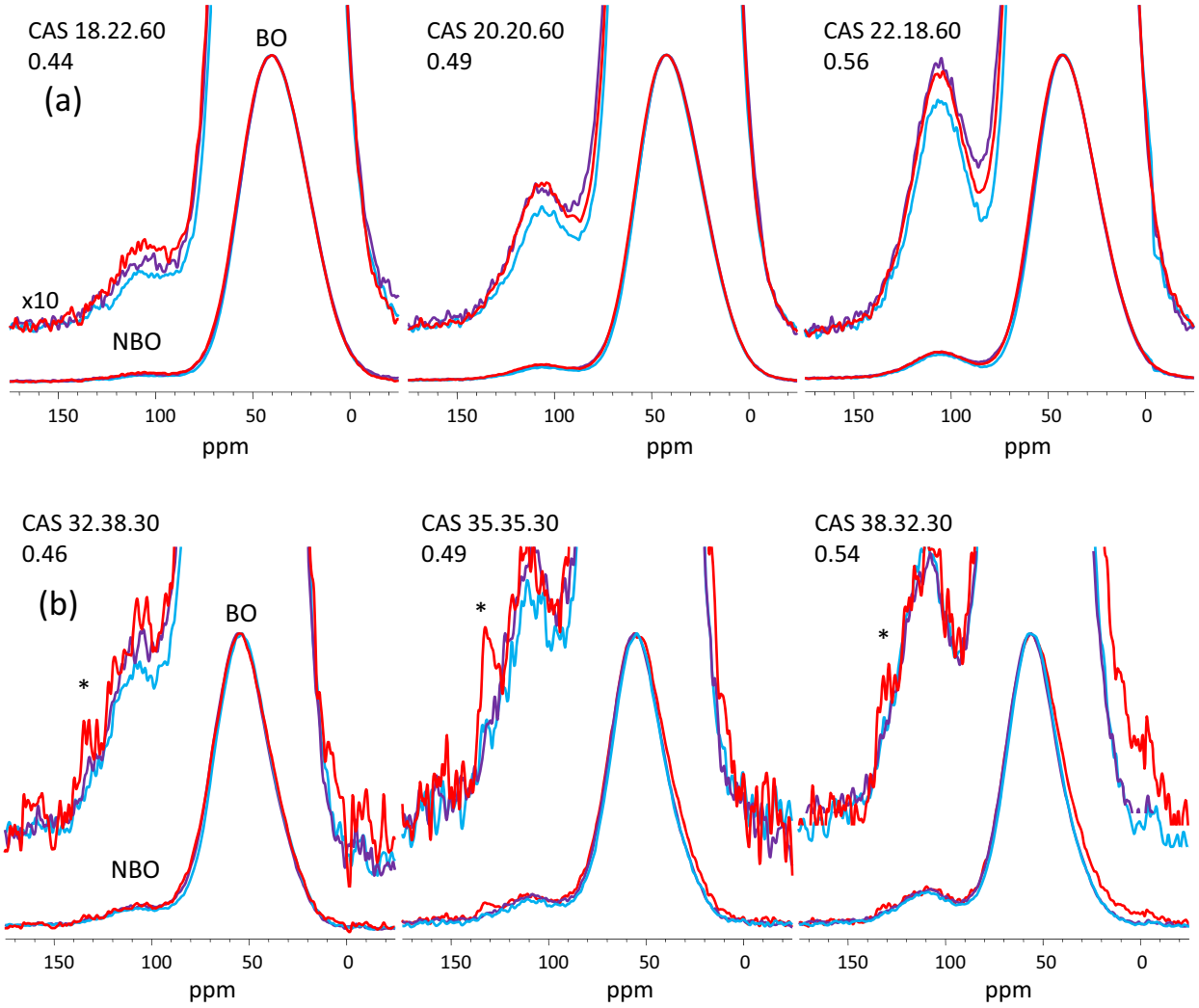
CAS 18.22.60
0.44
(a)
BO
x10
NBO
CAS 20.20.60
0.49
CAS 22.18.60
0.56
150
100
50
0
ppm
CAS 32.38.30
0.46
(b)
BO
*
NBO
CAS 35.35.30
0.49
CAS 38.32.30
0.54

Figure 1

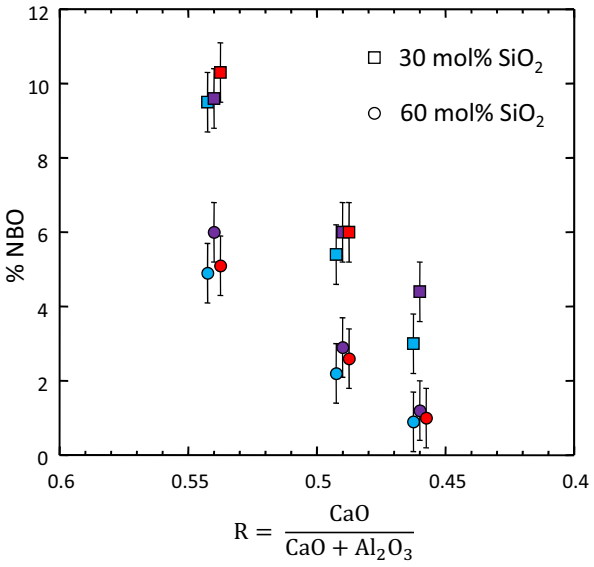
12
10
8
6
4
2
0
% NBO
30 mol% SiO2
60 mol% SiO2
0.6
0.55
0.5
0.45
0.4
R = CaO / (CaO + Al2O3)

Figure 2

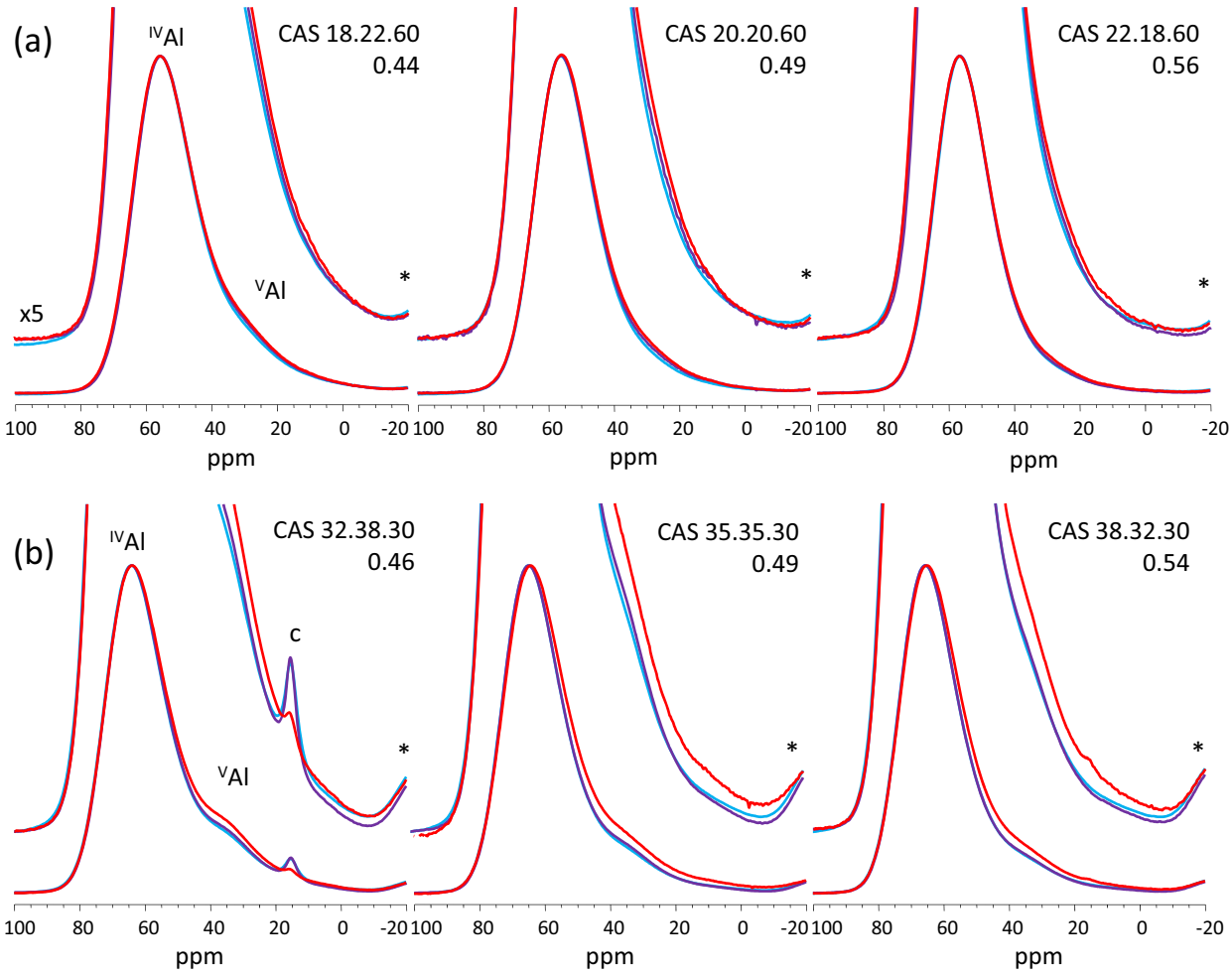
(a)
IVAl
CAS 18.22.60
0.44
VAl
x5
*
CAS 20.20.60
0.49
CAS 22.18.60
0.56
100 80 60 40 20 0 -20
ppm
(b)
IVAl
CAS 32.38.30
0.46
c
VAl
CAS 35.35.30
0.49
CAS 38.32.30
0.54

Figure 3

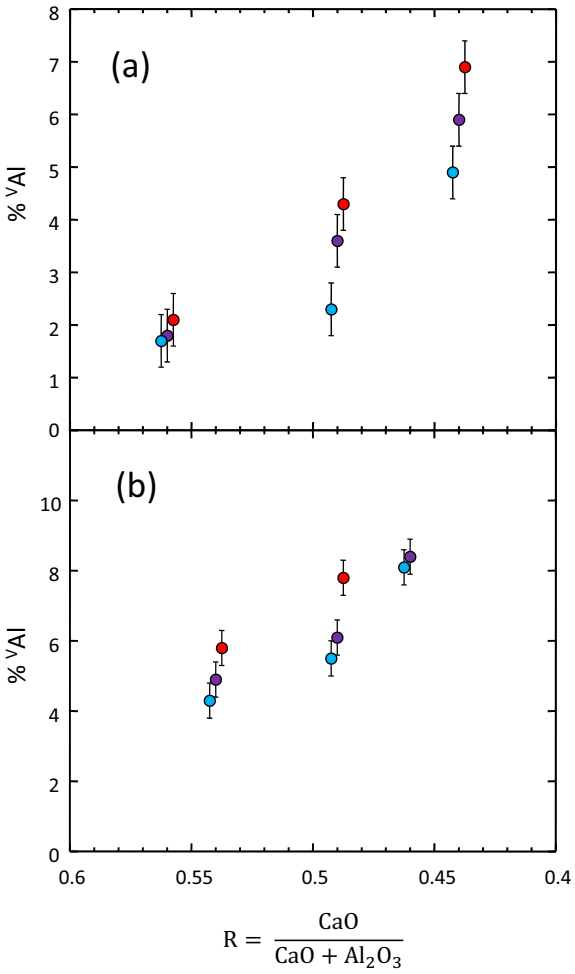

Figure 4